Development of a high-speed scanning micro PIV system using a rotating disc

K. P. Angele, Y. Suzuki, J. Miwa and N. Kasagi

The University of Tokyo, Tokyo 113-8656, Japan

E-mail: angele@thtlab.t.u-tokyo.ac.jp

Abstract. A novel high-speed scanning micro PIV system has been developed in order to provide time-resolved, pseudo-three-dimensional flow-field information. The focal plane is moved rapidly in the out-of-plane direction by changing the optical length using a rotating disc having glass windows with different thickness. In the present prototype system, the extent of the scanning depth is 50 μm, and the maximum scanning frequency is 100 Hz. Through a series of experiments in a two-dimensional micro channel, it was found that the velocity data are in good agreement with the analytical solution. The fluctuation in the flow rate delivered by a syringe pump is successfully measured with the present system. This demonstrates the applicability of the present scanning system for unsteady flow measurements.

Keywords: micro PIV, scanning, high-speed camera, rotating disc

Submitted to: *Meas. Sci. Technol.*

1. Introduction

Recently, micro thermal fluids systems such as micro total analysis system (μTAS) and micro energy conversion system (Power micro-electro-mechanical system, Power MEMS) have attracted much attention. Although the flow mostly remains laminar in micro conduits of such systems, physical experiments should still play an important role in the analysis of the flow field. For instance, bio-fluid flows often include cells or particles, and can exhibit non-Newtonian characteristics, for which numerical analysis sometimes becomes difficult. Furthermore, the cell diameter is often comparable to the channel size and consequently the velocity field is three-dimensional and unsteady.

With the recent development of micro particle image velocimetry (PIV), it has become possible to quantitatively measure the velocity field in micro channels; see e.g., Santigo *et al.* (1998); Meinhart *et al.* (1999); Kim *et al.* (2002); Devasenathipathy *et al.* (2003). Conventional micro PIV is essentially a two-dimensional measurement technique, with which the velocity field in a focal plane is obtained. On the other hand, scanning micro PIV systems, which are capable of measuring the velocity in different

sections of a flow, have also been proposed. In such, the objective lens is often moved in the out-of-plane direction using PZT drives, Shinohara *et al.* (2005). However, the scanning frequency is limited to about 10 Hz, which implies that they are not suitable for time-resolved measurements of rapidly varying flows, Kinoshita *et al.* (2005).

The aim of the present study is to overcome the above mentioned deficiency of current scanning systems and develop a scanning micro PIV system that can provide time-resolved, pseudo-three-dimensional flow-field information.

2. Experimental setup

a) b)

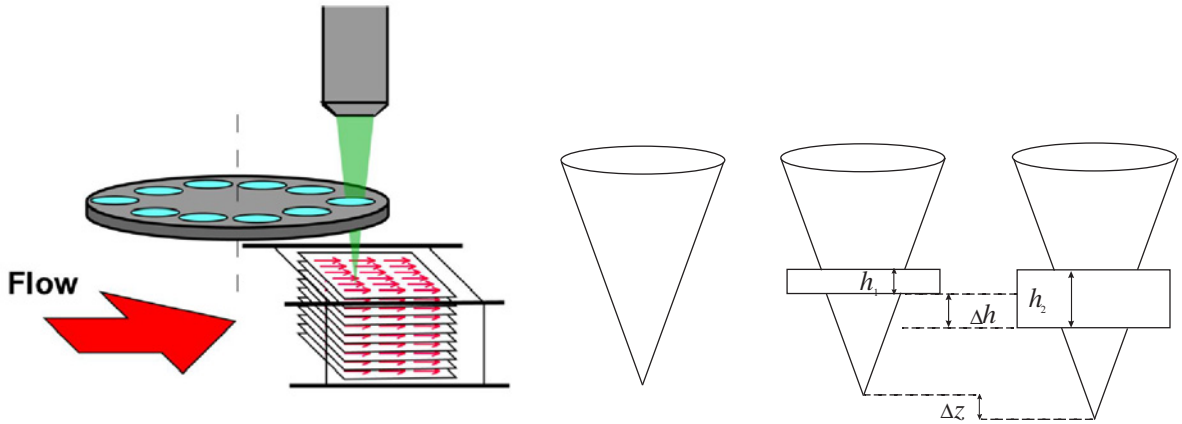

Figure 1. (a) Conceptual picture of the scanning micro PIV. (b) Glass windows having different thickness in order to vary the optical length.

To accomplish our aim, we employ a rotating disc with glass windows with different thickness in order to vary the optical length underneath the objective lens as shown in Figure 1(a). The displacement of the focal plane in the out-of-plane direction Δz is determined by the difference in the optical length, see Figure 1(b). When the difference in thickness of two subsequent glass windows is Δh, Δz is given by $\Delta h(1\text{-}n_0/n_1)$ according to Snell's law, where n_0=1 (air) and n_1=1.5 (glass). With the present configuration, the scanning disc has ten small glass windows with a thickness ranging from 500 μm to 625 μm, with Δh=12.5 μm, so that Δz is 5 μm when measuring in water. The uncertainty in the glass thickness is less than 1μm. The positions of the focal plane were investigated by traversing a slide-glass with fluorescent particles in the in-depth direction using a micro high-precision stage. The accuracy of the position of each measurement plane is within what can be determined with the micro stage (1 μm). Unlike conventional scanning systems, the locations of the focal plane are well defined by the thickness of the glass window, and the scanning depth can be made much larger. Moreover, the scanning frequency can be much higher regardless of the scanning depth. The disk rotates with the aid of a DC motor and the rotation speed can be varied. In

the present experiments, the disc rotates at 6000 rpm, which corresponds to a scanning frequency of 100 Hz. The uncertainty in the rotation speed of the scanning disc is about 15 rpm at 6000 rpm.

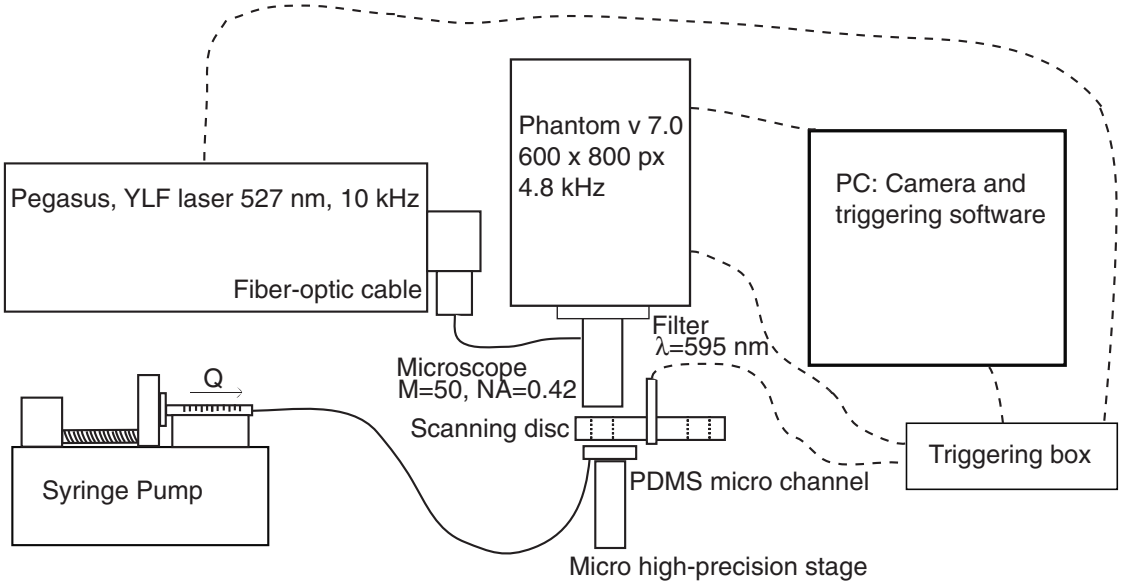

Figure 2. A schematic picture of the experimental setup.

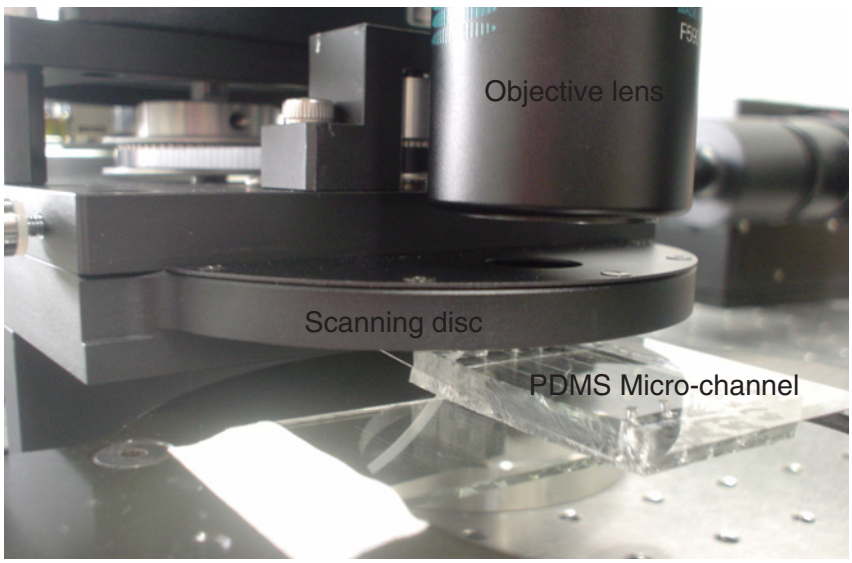

Figure 3. A close-up view of the optical setup.

Figure 2 shows a schematic picture of the experimental setup. We employ an optical setup designed for micro PIV (Seika Corp.), equipped with an objective lens with a magnification M of 50 and a numerical aperture NA of 0.42. It has a relatively large

working distance, which allows us to integrate the rotating scanning disc in between the objective lens and the micro channel at the expense of somewhat low NA, as shown in Figure 3.

A two-dimensional micro channel is used as the test section in the present flow measurement. The micro channel is made of PDMS, fabricated by conventional soft lithography techniques Xia & Whitesides (1998). A cover glass is bonded to the PDMS after oxygen plasma treatment to cover and seal the micro channel. The micro channel is 200 μm in width and 60 μm in depth. The accuracy of the channel height and width is within about 1% of the designed value. Particle images were taken through the cover-glass side, to avoid absorption of light in the PDMS. A syringe pump (Harvard 22, Harvard Apparatus) provides a nominally-constant flow rate of water. The water is kept at a constant temperature of 24°C throughout the experiments.

A high-speed CMOS camera (Phantom VII, Vision Research) was employed for capturing particle images. Each particle image contains 600 × 800 pixels, which renders a spatial resolution of 0.5 μm/pixel in the present setup.

A high-repetition-rate double-cavity YLF laser (Pegasus, New Wave Research) with a wavelength of 527 nm was used for whole-field illumination. The laser and the camera were synchronized with the rotating disc using a trigger unit (Labsmith LC880).

The Phantom is able to run up to 4800 Hz and the laser to 10000 Hz, however at reduced power, so the rotation speed of the scanning disc is the limiting device in the present system.

Pink fluorescent particles (Duke Scientific) with a diameter of 1 μm and a volume concentration of 0.1% were used as seeding. The excitation and emission peaks in the wavelength spectra of the particles are located at 542 nm and 612 nm, respectively. The high-pass filter has a cut-off wavelength at 595 nm. Figure 4 shows a raw particle image.

Willert *et al.* (1996) showed that random errors due to poor light intensity became significant once the dynamic range in the light intensity was below four bits. The maximum light intensity in the present images is of the order of eight bits. However, the level of background noise is significant due to the somewhat large focal depth as is indicated by the raw particle image. The effect of image quality will be further discussed in section 3.2.1 and 3.2.2.

The time difference between successive images can be made as low as 10 μs when two laser pulses are introduced to the same focal plane in one scanning cycle. In the present experiment, the flow velocity is very low and a single laser pulse is applied for each focal plane at a repetition rate of 1 kHz. Ten different wall-normal measurement positions are scanned in one cycle and hence Δt=10 ms.

According to Meinhart *et al.* (1999), the diameter of a particle image is given by $d_e = (d_s^2 + M^2 d_{phys.}^2)^{1/2}$, where $d_s = 2.44(1+M)\lambda NA^{-1}$ is the diameter of the diffraction limited point-spread function. With the present microscope (M=50, NA=0.42), laser (λ=527 nm) and physical particle size ($d_{phys.}$=1 μm), d_e=92.7 μm, which corresponds to approximately 5.6 pixels.

A Gaussian peak-fit was used for the sub-pixel interpolation as recommended by

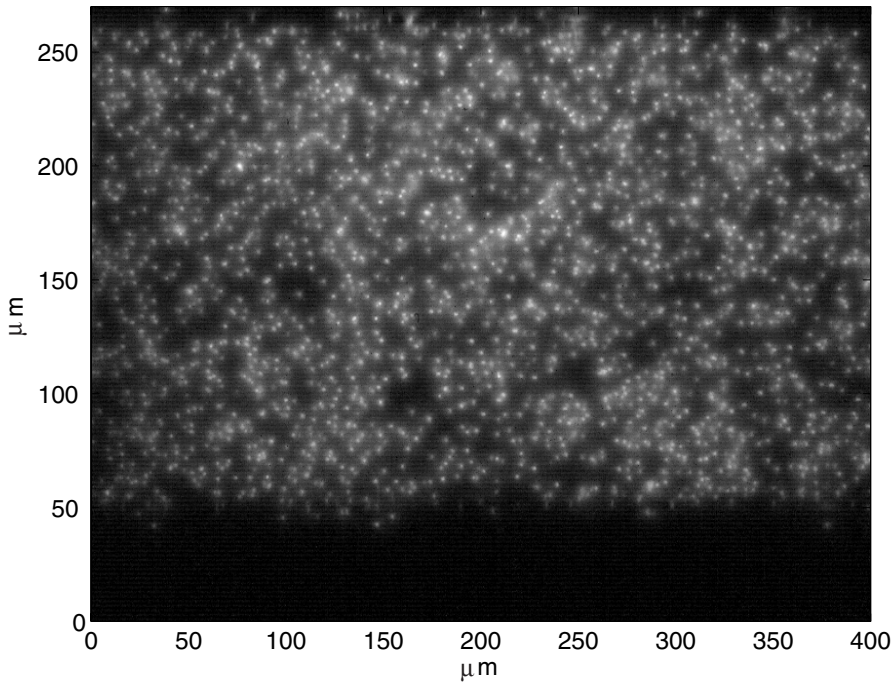

Figure 4. A raw particle image at the centerline of the micro channel when using the scanning disc.

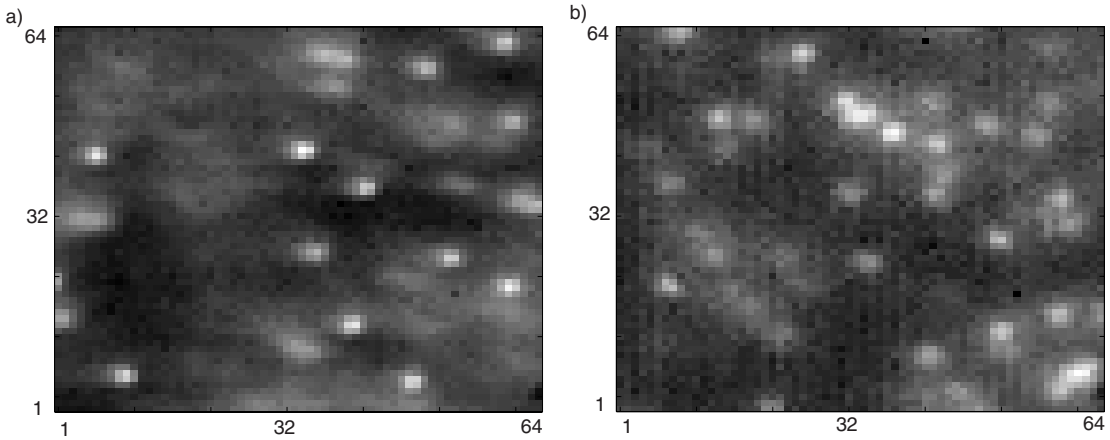

Figure 5. A sub-region of a particle image with the same size as the interrogation area but square, 64 × 64 pixels. (a) Without the scanning disc (b) with the scanning disc.

Willert *et al.* (1996) and Westerweel (1997) in order to minimize the effects of peak-locking. Other PIV setup parameters were designed according to the criteria given by Angele & Muhammad-Klingmann (2005) to minimize errors in the velocity statistics introduced by peak-locking.

The focal depth, which defines the measurement volume, is roughly 10 μm based

on the estimations given by Meinhart *et al.* (2000), Wereley *et al.* (2002) and Kim *et al.* (2002). The depth of correlation, given by Olsen & Adrian (2000), is similar in magnitude. This rather large fraction of the channel depth is a consequence of the low NA.

Keane & Adrian (1992) examined the error due to a velocity gradient across the IA and they suggested a criteria as $0.5\Delta U\Delta t/\Delta z \leq 0.03$. With the present settings, this criteria corresponds to $\Delta U \leq 0.06$ mm/s at Q=0.1 μl/min. Errors due the velocity gradient will be further discussed in section 3.3.

The images were evaluated by a modified version of a MATLAB-based software (MATPIV), which was developed by Sveen (2004). The cross-correlation technique was applied using elongated interrogation areas (IAs) of 16 $\times$ 256 pixels in the wall-normal and streamwise directions respectively with an overlap of 50%. This gives us 74 $\times$ 5 velocity vectors in each image. The number of particles in each IA is estimated to be about 25, see Figure 5. This is well above the recommendations of 5$-$10 by Keane & Adrian (1992).

As a means of detecting spurious vectors we employ the peak value ratio (PVR), which is the ratio between the highest and the second highest peaks in the correlation plane. The lower limit recommended by Keane & Adrian (1992) is PVR=1.2. We also discard negative velocities and velocities which were larger than the centerline velocity.

Vibrations induced by the rotating disc were estimated by capturing images of a slide-glass with steady particles. It was found that the root-mean-square value of the displacement is about 0.1 pixels, which is of the order of the accuracy of the PIV evaluation technique.

The effect of Brownian motion on the measured velocity was estimated to be 0.13% using the expression given by Santigo *et al.* (1998), and can be neglected in the present experiment.

3. Results

3.1. A direct comparison to conventional micro PIV

The effect of introducing the scanning disc on the quality of the PIV data was investigated by a direct comparison to a conventional micro PIV measurement. The measurements were carried out at the centerline of the channel under a steady flow condition with a flow rate of 0.2 μl/min. As shown in Figure 6(a), the ensemble-averaged PVR is decreased by 23% when the scanning disc is introduced. Despite of that, the data for the mean velocity agrees well with the analytical solution also for the scanning micro PIV system, as is shown in Figure 6(b). The u_{rms}/U_{cl} is of the order of 3% in both cases.

The PVR of a correlated pair of particle images in PIV can be affected by various experimental conditions. Keane & Adrian (1992) report that a velocity gradient across the IA and an insufficient number of particles in the IA can decrease the PVR. The

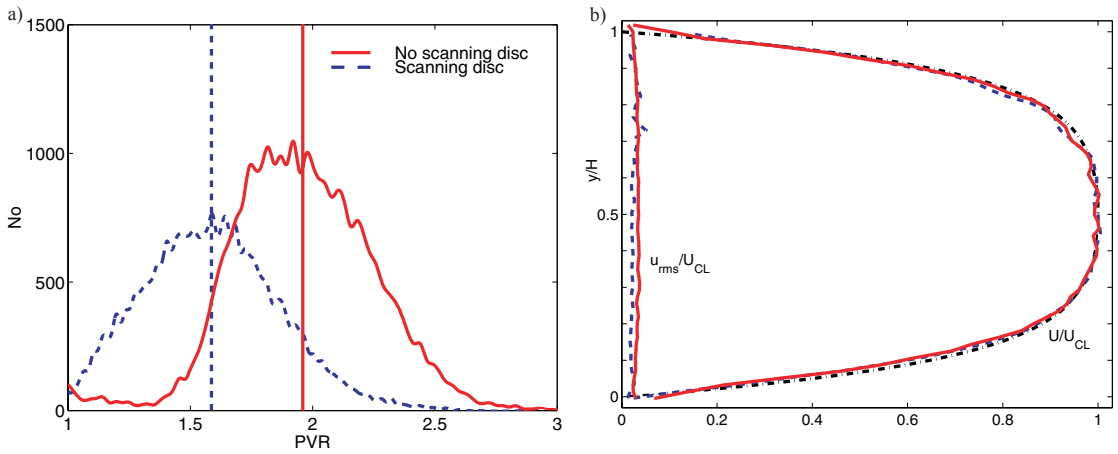

Figure 6. (a) The PDFs of the PVR for all spanwise positions with and without the scanning disc. The vertical lines correspond to the mean values. (b) The normalized streamwise mean velocity and fluctuations with and without the scanning disc. The analytical solution for the streamwise velocity is indicated by (— · —).

PVR can also be deteriorated by an insufficient displacement of the particles in terms of pixels, and by the particle image diameter in terms of pixels, Westerweel (1997). Willert *et al.* (1996) report that a poor dynamic range in the light intensity can also cause a decrease in the PVR. The three former parameters are identical in the two experiments with and without the scanning disc. Therefore, the reduction in the PVR with the scanning disc should be attributed to the change in the particle image quality (particle image diameter and light intensity with respect to the light intensity of the background noise).

Although it is difficult to evaluate the quality of individual particles, it is obvious that the overall light intensity of the particle images is reduced when inserting the scanning disc. It also appears that the particle images are not as well-defined as in the case without the scanning disc, i.e. they become slightly blurred or defocused.

3.2. Reduced image quality due to the scanning disc

3.2.1. Defocusing effect A micro pattern, consisting of a circle with a diameter of 100 μm, was illuminated with white light and its image was captured with and without the presence of the scanning disc. This allows us to investigate a possible defocusing effect of the scanning disc. The position of the focal plane was determined subjectively by observing the sharpness of the image while traversing the micro stage in steps of 1 μm (10% of the focal depth) in the depth-of-field direction. Figure 7(a,b) shows a part of the circle, which appears as dark on a white background. One can observe how the edge of the circle becomes defocused when introducing the scanning disc. Figure 7(e) displays the light intensity across the edge of the pattern. The range in the light intensity is decreased for the image with the scanning disc, which implies a less sharp transition across the edge of the circle. This suggests a defocusing effect when introducing the

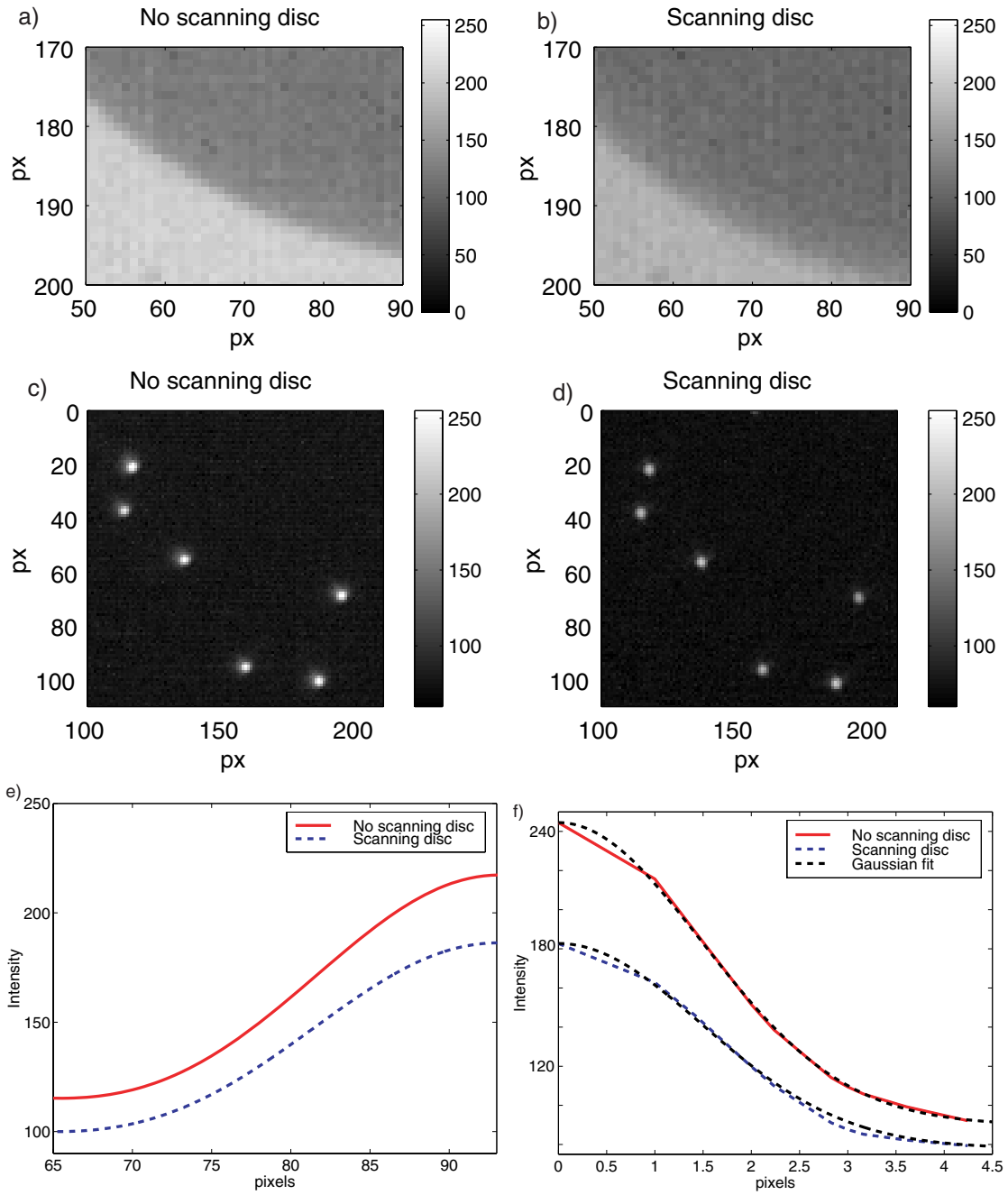

Figure 7. (a,b) Circular micro-pattern. (c,d) Particles on a slide-glass. (e) Average light intensity distribution across the edge of the circular micro-pattern. (f) Average light intensity distribution of the fluorescent particles on a slide-glass.

scanning disc.

Another image was captured with fluorescent particles on a slide-glass in order to estimate how individual particles are affected by introducing the scanning disc. The particles were illuminated with laser and photographed with and without the presence

of the scanning disc. A sub-region of these images are shown in Figure 7(c,d). It is obvious that the light intensity is overall decreased. A local maximum in the light intensity was taken as the center of a particle. The same particles were detected with and without the scanning disc, and the average light intensity distribution for a particle was computed. Figure 7(f) shows the light intensity distribution in the radial direction. It is confirmed that the light intensity is overall decreased when inserting the scanning disc. The maximum light intensity is reduced by 25%, which is in line with the result from the channel flow experiment. The shape of the particle images is approximately Gaussian for both cases and the particle image diameter, taken as the location where the intensity is e^{-2} of the maximum intensity, is about 5.9 pixels for both cases. This is in line with the estimate using the expression given by Meinhart *et al.* (1999), see section 2.

3.2.2. Synthetic particle image simulations It is a well-established technique to use synthetic particle images in order to investigate the effect of image quality on the calculated velocity field, Okamoto *et al.* (2000). In order to investigate if the observed defocusing effect, which leads to a reduction in the particle image light intensity, could be the reason for the reduced PVR, synthetic particle images were generated and evaluated through pseudo PIV measurements. The image size was 256×256 pixels and the IA size was the same as in the experiment, i.e. 16×256 pixels. A two-dimensional channel flow was imposed with a center line velocity that corresponds to a maximum displacement of 5 pixels. Only half the channel in the spanwise direction was simulated. The number of image pairs was enough to assure that the statistical error in the PVR is below 1%. The particle positions were randomly distributed in the virtual image plane and in the depth-of-field direction. The particle image intensity distribution in the image plane is assumed to be Gaussian and the maximum intensity depends on the position in the laser sheet in the depth-of-field direction. The light intensity of the virtual laser sheet is assumed to be homogenous in the image plane. Its extent in the depth-of-field direction is 2.5 pixels and the intensity distribution is assumed to be Gaussian. The average particle image diameter d_p was varied between 2 and 16 pixels. The particle diameter in each case varies randomly with an rms of 1 pixel. The number of particles in the IA (NOP) was varied between 8 and 64. The maximum light intensity I_{max} was varied between 2 and 26. Random background noise $I_{backgr.}$ was added to the whole image plane. It has a uniform distribution in the interval zero to one and is un-correlated for the two images used for calculating the velocity field. The ratio $I_{max}/I_{backgr.}$ was calculated as the maximum intensity divided by the maximum in the background noise.

Figure 8(a) shows the ensemble-averaged PVR based on all spanwise positions for d_p=6 pixels as a function of $I_{max}/I_{backgr.}$ for different NOP. It can be seen that there is little benefit of increasing $I_{max}/I_{backgr.}$ beyond four bits (=16), in line with the results by Willert *et al.* (1996). On the other hand, when $I_{max}/I_{backgr.}$ decreases below 16, there is a drastic decrease in the PVR. When decreasing the NOP, there is an overall decrease in the PVR in line with the results by Keane & Adrian (1992).

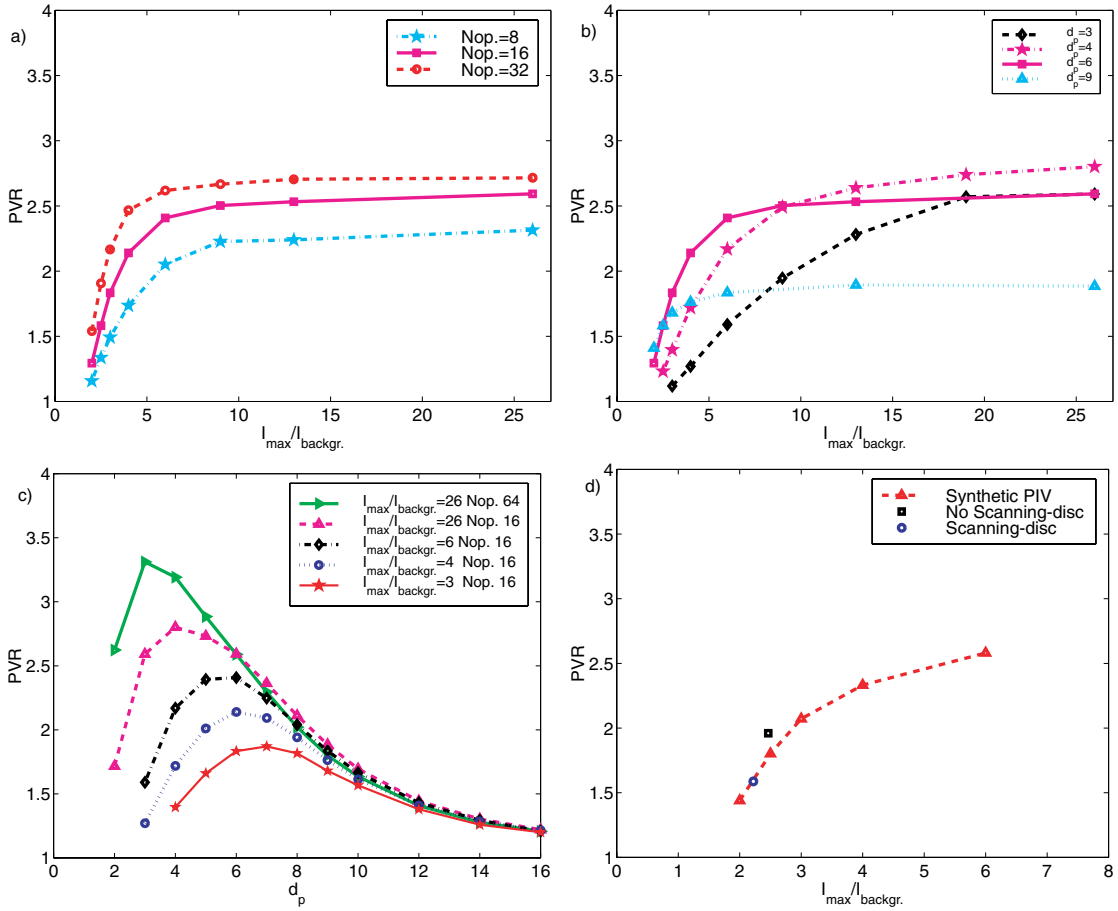

Figure 8. Simulation result of the sensitivity in the PVR to image quality. (a) The ensemble-averaged PVR for d_p=6 as a function of the $I_{max}/I_{backgr.}$ for different NOP. (b) The ensemble-averaged PVR for NOP=16 as a function $I_{max}/I_{backgr.}$ for different d_p. (c) The ensemble-averaged PVR as a function of d_p for different NOP and $I_{max}/I_{backgr.}$. (d) A comparison between the simulation and the experimental data with and without the scanning disc for NOP=25, d_p=5.9.

Figure 8(b) shows the ensemble-averaged PVR for NOP=16 as a function of $I_{max}/I_{backgr.}$ for different d_p. It can be seen that the critical value for $I_{max}/I_{backgr.}$ and the asymptotic value of the PVR strongly depends on d_p.

Figure 8(c) shows the ensemble-averaged PVR as a function of d_p for different NOP and $I_{max}/I_{backgr.}$. When the NOP and $I_{max}/I_{backgr.}$ are sufficiently high, there is a maximum in the PVR around d_p=3 pixels, in line with Westerweel (1997). When decreasing NOP and $I_{max}/I_{backgr.}$ the PVR is overall decreased and the optimal particle image diameter is shifted towards higher values.

Figure 8(d) shows a comparison between the present simulation and the experimental data with and without the scanning disc. The NOP used for the simulation was estimated from the raw PIV images and is 25. The mean particle image diameter used in the simulation was taken as 5.9 pixels for both cases based on the results

presented in Figure 7(f). The maximum intensities in the experiment were taken as the ensemble-average of the instantaneous maximum for all images. The values of the background noise in the experiments were taken as the ensemble-average of the light intensity in the whole image. The experimental data are in good agreement with the simulation result. This indicates that the reduction in the PVR should be attributed to the reduced particle image light intensity.

3.3. Steady, quasi three-dimensional measurements

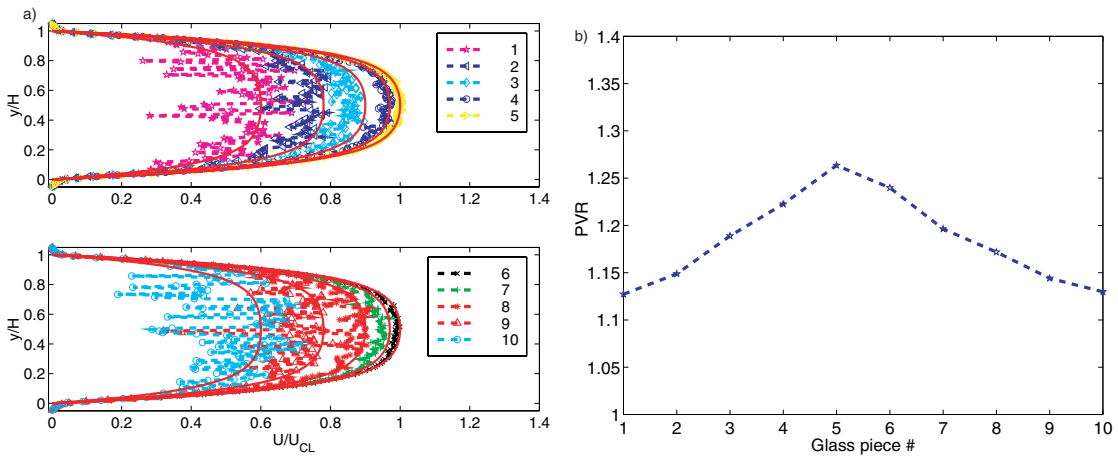

Figure 9. (a) The normalized streamwise mean velocities at all measurement planes through out the entire depth of the channel. The numbering corresponds to the measurement planes, where 1 is closest to the top wall. (b) The PVR at all measurement planes through out the entire depth of the channel.

Figure 9(a) displays the mean velocity profiles throughout the entire depth of the channel. It is obvious that the scatter in the data increase closer to the top and bottom walls of the channel. Figure 9(b) indicates that the ensemble-averaged PVR at each wall-normal location (based on all the spanwise positions) decreases towards the top and bottom walls of the channel. This is most likely due to the fact that the velocity gradient across the focal plane increases with a decreasing distance to the top and bottom walls of the channel. This problem will be overcome in the future by integrating the scanning disc above the objective lens, which allows for the use of a larger NA lens, which significantly reduces the focal depth. An alternative would be to make use of the confocal scanner technique reported by Park *et al.* (2004) in order to reduce the focal depth.

3.4. Unsteady, quasi three-dimensional measurements

Finally, measurements under unsteady flow conditions were carried out in order to demonstrate the ability of the scanning system for quasi-three dimensional temporally-resolved measurements. The flow rate was lowered to 0.1 μl/min in order to decrease

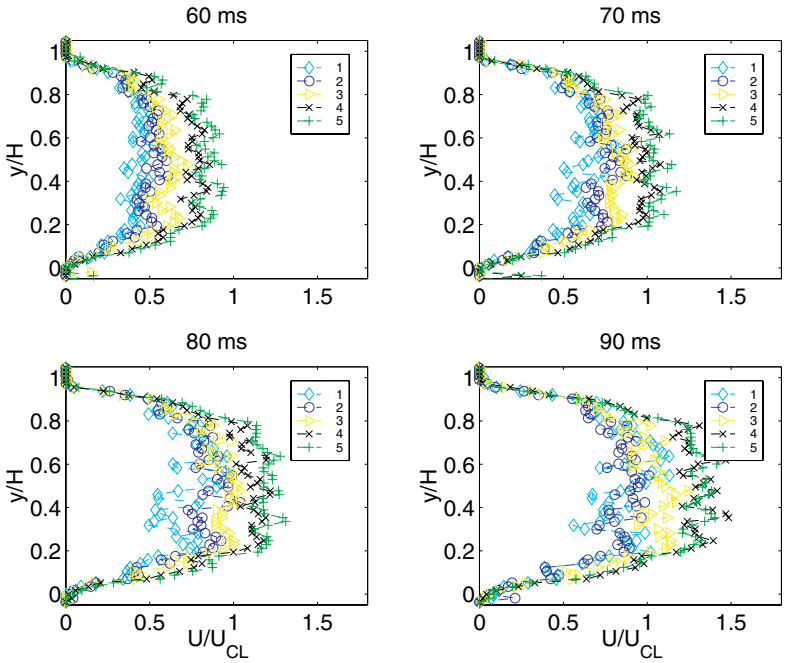

Figure 10. The instantaneous velocity profiles for four successive scans taken at a scanning rate of 100 Hz (note that only the results from the upper half of the channel are displayed to increase the visibility).

the problem with the velocity gradient. However, this increases the influence of random errors since the particles are moving a shorter distance in terms of pixels. Figure 10 shows instantaneous velocity distributions for four successive scans taken at a scanning rate of 100 Hz. The variation in the magnitude of the velocities is obvious.

The flow rate was estimated by integrating the instantaneous velocity profiles at the ten measurement planes throughout the entire depth of the channel. Figure 11 shows the time trace of estimated flow rate. Although the nominal flow rate is kept constant at 0.1 μl/min, the instantaneous flow rate delivered by the present syringe pump has a large fluctuation with a typical frequency of the order of 3 Hz. This result demonstrates the ability of the present system for unsteady flow measurements.

4. Discussion

The results reported here indicate that the present technique is very powerful for unsteady quasi three-dimensional measurements of micro flows. However, the system still requires some improvements. The careful investigation of the sources of noise clearly indicates that the noise can be attributed to the reduced particle image light intensity, when introducing the scanning disc. This can perhaps be overcome by using a more powerful laser. Another source of noise is the velocity gradient across the rather large focal depth. The noise in the data at the center line is very low and the reduction in the PVR and the increase in the noise is well correlated with the distance from the center

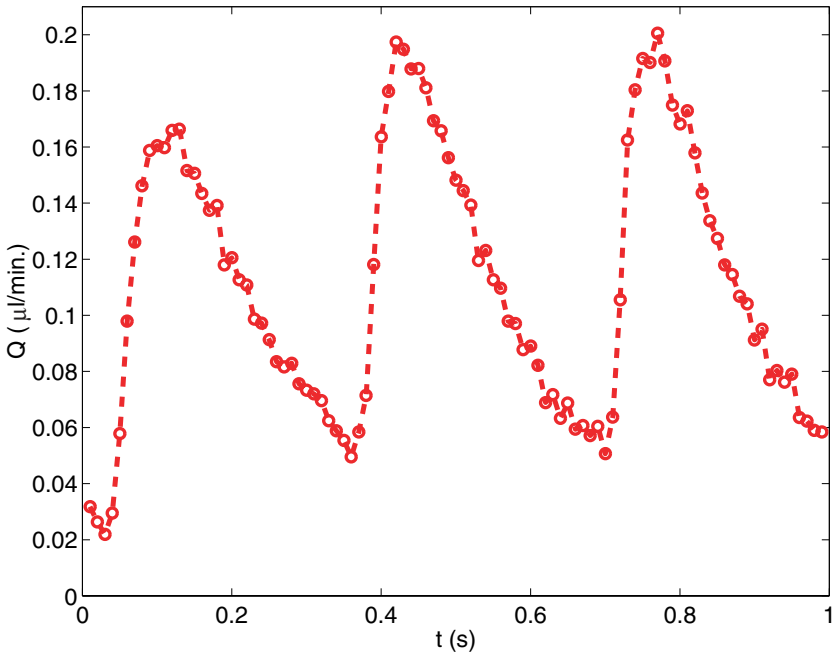

Figure 11. Measured unsteady flowrate delivered by the syringe pump at a nominal flow rate of 0.1 μl/min.

line. This problem will be overcome in the future by integrating the scanning disc above the objective lens. This allows for the use of a lens with a larger NA, which significantly reduces the focal depth. Another alternative might be to incorporate a confocal scanner in order to reduce the focal depth, as reported by Park *et al.* (2004).

5. Conclusions

A novel high-speed scanning micro PIV system has been developed and evaluated through a series of experiments. It was demonstrated that it can provide time-resolved, pseudo-three-dimensional flow field information. The experimental data taken in a micro channel compare well with the analytical solution and the data measured with conventional micro PIV. It was found that the signal-to-noise ratio (PVR) is somewhat deteriorated for the scanning micro PIV. This can be attributed to a defocusing effect caused by the glass windows on the scanning disc.

Acknowledgments

This work is supported by Grant-in-aid for Scientific Research (S) (No. 15106004) and the 21^{st} COE Program "Mechanical Systems Innovation" from JSPS.

References

Angele, K. & Muhammad-Klingmann, B. 2005 A simple model for the effect of peak-locking on the accuracy of boundary layer turbulence statistics in digital PIV. *Exp. Fluids* **38 (3)**, 341–347.

Devasenathipathy, S., Santiago, J. G., Wereley, S. T., Meinhart, C. D. & Takehara, K. 2003 Particle imaging techniques for microfabricated fluidic systems. *Exp. Fluids* **34**, 504–514.

Keane, R. & Adrian, R. 1992 Theory of cross-correlation in PIV. *Appl. Sci. Research* **49**, 191–215.

Kim, M. J., Beskok, A. & Kihm, K. D. 2002 Electro-osmosis-driven micro-channel flows: A comparative study of microscopic particle image velocimetry measurements and numerical simulations. *Exp. Fluids* **33**, 170–180.

Kinoshita, H., Oshima, M., Kaneda, S. & Fujii, T. 2005 Confocal micro-PIV measurement of internal flow in a moving droplet. *Micro-TAS 2005* **1**, 629–631.

Meinhart, C. D., Wereley, S. T. & Gray, M. H. B. 2000 Volume illumination for two-dimensional particle image velocimetry. *Meas. Sci. Technol.* **27**, 414–419.

Meinhart, C. D., Wereley, S. T. & Santigo, J. G. 1999 PIV measurements of a microchannel flow. *Exp. Fluids* **27**, 414–419.

Okamoto, K., Nishino, S. & Kobayashi, T. 2000 Standard images for particle-image velocimetry. *Meas. Sci. Technol.* **11**, 685–691.

Olsen, M. G. & Adrian, R. J. 2000 Out-of-focus effects on particle image visibility and correlation in microscopic particle image velocimetry. *Exp. Fluids* **29**, S166–S174.

Park, J. S., Choi, C. K. & Kihm, K. D. 2004 Optically sliced micro-piv using confocal laser scanning microscopy (CLSM). *Exp. Fluids* **37**, 105–119.

Santigo, J. G., Wereley, S. T., Meinhart, C. D., Beebe, D. J. & Adrian, R. J. 1998 A particle image velocimetry system for microfluidics. *Exp. Fluids* **25**, 316–319.

Shinohara, K., Sugii, Y., Jeong, J. & Okamoto, K. 2005 Development of 3D scanning micro particle image velocimetry system using a piezo actuator. *Rev. Sci. Instrum.* **76**, 106–109.

Sveen, J. K. 2004 An introduction to matpiv v.1.6.1. Eprint no. 2, **ISSN** 0809-4403, Dept. of Mathematics, University of Oslo, http://www.math.uio.no/~jks/matpiv.

Wereley, S. T., Gui, L. & Meinhart, C. D. 2002 Advanced algorithms for microscale particle image velocimetry. *AIAA J.* **40** (6), 1047–1055.

Westerweel, J. 1997 Fundamentals of digital particle image velocimetry. *Meas. Sci. Technol.* **8**, 1379–1392.

Willert, C., Raffel, M., Kompenhans, J., Stasicki, B. & Kähler, C. 1996 Recent applications of Particle Image Velocimetry in aerodynamic research. *Flow Meas. Instrum.* **7** (3/4), 247–256.

Xia, Y. & Whitesides, G. M. 1998 Soft lithography. *Angew. Chem. Int. Ed.* **37**, 550–575.